A&A 521, A56 (2010)
DOI: 10.1051/0004-6361/200913275

Astronomy & Astrophysics

Trend of photospheric magnetic helicity flux in active regions generating halo coronal mass ejections⋆

A. Smyrli[1,2], F. Zuccarello[1], P. Romano[3], F. P. Zuccarello[4], S. L. Guglielmino[1], D. Spadaro[3], A. W. Hood[2], and D. Mackay[2]

[1] Dipartimento di Fisica e Astronomia – Sezione Astrofisica, Università di Catania, via S. Sofia 78, 95123 Catania, Italy
e-mail: emilia@oact.inaf.it
[2] Institute of Mathematics, University of St. Andrews, The North Haugh, St. Andrews, Fife KY 169SS, Scotland, UK
[3] INAF – Osservatorio Astrofisico di Catania, via S. Sofia 78, 95123 Catania, Italy
[4] Centre for Plasma Astrophysics, K. U. Leuven, Celestijnenlaan 200B, 3001 Leuven, Belgium

Received 10 September 2009 / Accepted 22 April 2010

ABSTRACT

Context. Coronal mass ejections (CMEs) are very energetic events ($\sim 10^{32}$ erg) initiated in the solar atmosphere, resulting in the expulsion of magnetized plasma clouds that propagate into interplanetary space. It has been proposed that CMEs can play an important role in shedding magnetic helicity, avoiding its endless accumulation in the corona.
Aims. The aim of this work is to investigate the behavior of magnetic helicity accumulation in sites where the initiation of CMEs occurred to determine whether and how changes in magnetic helicity accumulation are temporally correlated with CME occurrence.
Methods. We used MDI/SOHO line-of-sight magnetograms to calculate magnetic flux evolution and magnetic helicity injection in 10 active regions that gave rise to halo CMEs observed during the period 2000 February to 2003 June.
Results. The magnetic helicity injection does not have a unique trend in the events analyzed: in 40% of the cases it shows a large sudden and abrupt change that is temporally correlated with a CME occurrence, while in the other cases it shows a steady monotonic trend, with a slight change in magnetic helicity at CME occurrence.
Conclusions. The results obtained from the sample of events that we have analyzed indicate that major changes in magnetic helicity flux are observed in active regions characterized by emergence of new magnetic flux and/or generating halo CMEs associated with X-class flares or filament eruptions. In some of the analyzed cases the changes in magnetic helicity flux follow the CME events and can be attributed to a process of restoring a torque balance between the subphotospheric and the coronal domain of the flux tubes.

Key words. Sun: activity – Sun: coronal mass ejections (CMEs) – magnetic fields

1. Introduction

Coronal mass ejections (CMEs) are sudden expulsions of magnetized plasma clouds from the solar atmosphere into the interplanetary medium. They are usually observed by coronagraphs above the occulting disk in projection on the plane of the sky, and therefore their connection to the magnetic region where they were initiated is not straightforward. In many cases, a twisted flux tube ejected in a CME appears in interplanetary space as a magnetic cloud in which the twisted nature remains well observable (Qiu et al. 2007; Longcope et al. 2007).

Depending on the velocity and acceleration values, it is possible to distinguish between two different classes of CMEs: a) *gradual* CMEs, characterized by velocities $v \sim 400$–600 km s^{-1} and gradual acceleration ($a \sim 3$–40 m s^{-2} within a distance from the Sun less than $\sim 30\ R_\odot$), generally associated with eruptive quiescent filaments; b) *impulsive* CMEs with higher initial velocities, in the range ~ 750–1000 km s^{-1}, and decelerating at distances $\sim 2\ R_\odot$ (Sheeley et al. 1999), generally associated with flares and eruptive active region filaments.

MacQueen & Fisher (1983) suggested that the reason for this different dynamical behavior might be due to a different driver mechanism (or at least one with a different strength): gradual CMEs, which are events associated to eruptive prominence, are supposed to undergo a significant net propelling force over extended periods, while impulsive CMEs, which are flare-associated events, are supposed to arise from an impulsive input into the low corona (see also Low & Zhang 2002; Chen & Krall 2003).

Although several models for the initiation of CMEs have been developed (see e.g. Forbes 2000), there is a lack of observational evidence to provide the necessary constraints. In the breakout model (Antiochos et al. 1999) a quadrupolar flux distribution is considered consisting of an overlying arcade whose flux is oppositely directed with respect to the underlying central arcade and two lateral flux systems. In this scenario the emergence of new magnetic flux (Zuccarello et al. 2008) and/or the shearing motions along the magnetic inversion line eventually result in a CME. Priest & Forbes (1990) and Forbes & Priest (1995) showed that within a bipolar topology, converging motions can result in the loss of equilibrium of a magnetic flux-rope leading to a catastrophic eruption. Chen & Shibata (2000) showed that the injection of new magnetic flux from below the photosphere is also responsible for the eruption of a pre-existing flux-rope. More global MHD simulation of the emergence of a twisted flux tube have been carried out by Archontis & Török (2008). The authors found that a flux rope is formed within the expanding field due to shearing and reconnection of field lines at

⋆ Appendix is only available in electronic form at http://www.aanda.org

low atmospheric heights. Depending on if the corona is magnetized or not, the expanding flux rope experiences a full eruption or remains confined.

A useful quantity to distinguish between these cases is the magnetic helicity. It provides a measure of the connection of the magnetic field lines within a volume and also quantifies how much a flux tube is twisted or a magnetic arcade is sheared (Berger 1984; Heyvaerts & Priest 1984; Pariat et al. 2006; Démoulin & Pariat 2009). It is one of the few global quantities which is conserved also in resistive magnetohydrodynamics (MHD), on a timescale much smaller than the global diffusion timescale. However, when CMEs release magnetic energy stored over a large volume, they lead to the partial opening of the magnetic field lines and, as a result, the helicity does not remain conserved in a volume on the active region scale. In particular, the amount of magnetic helicity that can be expelled during a CME can be estimated by the variation of coronal helicity in the active region that generates a CME.

In the recent simulations of Yeates & Mackay (2009), the authors carried out global simulations of the solar corona based on photospheric observations for a period of six months in 1999. The model included the effects of flux emergence, shearing by surface motions and cancellation along with the formation and ejection of flux ropes due to loss of equilibrium. By varying the rate at which magnetic helicity was injected, the model produced 50% of the observed CME rate over the simulated period (see also Mackay & van Ballegooijen 2006). In contrast to this model, Cook et al. (2009) studied the number and locations of coronal null points, a key element in the magnetic breakout model, over two solar cycles. They found that the number of nulls followed a cycle variation, peaking at maximum of 15–17 per rotation. The vast majority of null points were located above active latitudes and lay at low heights in the corona.

Coronal mass ejections are prime candidates for carrying away the accumulated helicity (Heyvaerts & Priest 1984; Low 1996). They also provide a mechanism for shedding the required amount of helicity to avoid the saturation of the mean field $\bar{B}$ to a value much lower than the equipartion field strength, estimated as 10^{46} Mx^2 per cycle from simulations (Brandenburg & Sandin 2004). Thus, it is crucial to estimate the amount of magnetic helicity that can be expelled during a CME, for instance by measuring the variation of coronal helicity in the active region that generates the CME.

Nindos & Andrews (2004) performed a statistical study of 133 big flares of M and X class and found that in the pre-flare phase the coronal magnetic helicity of active regions producing big flares not correlated with CMEs is smaller than the coronal magnetic helicity of active regions producing CME-associated big flares. Furthermore, Moon et al. (2002) found that an amount of magnetic helicity on the order of 10^{41} Mx^2 was impulsively injected into the corona around the peak time of four eruptive flares.

On the basis of these results it is clear that the study of the magnetic helicity evolution in active regions can provide a useful tool to obtain important information about the mechanisms able to produce instabilities in the magnetic configuration. Moreover, the investigation of the magnetic helicity trend, before and after a CME occurrence, might contribute to our understanding of the role effectively played by these events in any eventual change in the magnetic helicity accumulation process (see, e.g., Nindos et al. 2003).

In this regard it is important to make a distinction between two cases. The former is related with the change in magnetic helicity prior to the CME occurrence, which should be related with phenomena able to destabilize the coronal configuration, like new flux emergence or shearing/twisting of the magnetic field lines. The latter is related with changes in magnetic helicity occurring after the CME that, as suggested by Longcope & Welsh (2000) and Chae et al. (2003), might be due to the unbalance of torque between the sub-photospheric part of the flux rope and the coronal field which just lost some stress via the CME launch.

Therefore we determined here the evolution of both magnetic flux and magnetic helicity flux in active regions where a flare or a filament eruption occurred close in time with a halo CME to investigate the above mentioned scenarios.

The layout of this paper is as follows: in the next section we recall the definition of magnetic helicity and related parameters, in Sect. 3 we describe the data, the methods of analysis and the results, in Sect. 4 we present the discussion and our conclusions.

2. Magnetic helicity

Magnetic helicity is given by a volume integral

$$H = \int_V \boldsymbol{A} \cdot \boldsymbol{B}\, \mathrm{d}V, \tag{1}$$

where $\boldsymbol{A}$ is the magnetic vector potential and $\boldsymbol{B} = \nabla \times \boldsymbol{A}$ is the magnetic field. This definition of helicity is physically meaningful only when $\boldsymbol{B}$ is fully contained inside the volume V. However, our study is concerned with a coronal volume enclosing an active region, i.e. an open magnetic system. Berger & Field (1984) showed that under this constraint the quantity that better describes the system is the relative magnetic helicity, defined as

$$H_{\mathrm{rel}} = \int (\boldsymbol{A} + \boldsymbol{A}_{\mathrm{p}}) \cdot (\boldsymbol{B} - \boldsymbol{B}_{\mathrm{p}}) \mathrm{d}V, \tag{2}$$

where $\boldsymbol{B}$ is the magnetic field, $\boldsymbol{A}$ is the magnetic vector potential, $\boldsymbol{B}_{\mathrm{p}}$ is the potential magnetic field that has the same distribution as $\boldsymbol{B}$ at the boundary, and finally, $\boldsymbol{A}_{\mathrm{p}}$ is its corresponding vector potential, uniquely specified by the observed flux distribution on the surface with the equations

$$\nabla \times \boldsymbol{A}_{\mathrm{p}} \cdot \hat{\boldsymbol{n}} = B_{\mathrm{n}}, \qquad \nabla \cdot \boldsymbol{A}_{\mathrm{p}} = 0, \qquad \boldsymbol{A}_{\mathrm{p}} \cdot \hat{\boldsymbol{n}} = 0. \tag{3}$$

This relative magnetic helicity may vary due to the passage of magnetic field lines through the photospheric boundary (when the flux emerges), or through the sides (when the magnetic field expands to be in contact with neighboring active regions), or through the outer boundary (when a coronal mass ejection occurs). Unlike the magnetic helicity of fully enclosed magnetic fields, the helicity of open magnetic fields may change with time as it is transported through the boundaries. In this regard, it is worthwhile mentioning that most of the helicity injection in an active region occurs during magnetic flux emergence (Tian & Alexander 2008).

Therefore, the magnetic helicity in the coronal volume of an active region is a function of time. In order to determine this time variation, it is possible to use the following equation for the helicity flux (or injection rate) $\mathrm{d}H/\mathrm{d}t$ through a planar surface S_{p} (indicating the photospheric portion of the surface S bounding the volume V) (Berger and Field, 1984)

$$\frac{\mathrm{d}H}{\mathrm{d}t} = -2 \int_{S_{\mathrm{p}}} \left[(\boldsymbol{v}_{\mathrm{t}} \cdot \boldsymbol{A}_{\mathrm{p}})\, B_{\mathrm{n}} - (\boldsymbol{A}_{\mathrm{p}} \cdot \boldsymbol{B}_{\mathrm{t}})\, v_{\mathrm{n}} \right] \mathrm{d}S, \tag{4}$$

where the magnetic field $\boldsymbol{B}$ and the velocity field $\boldsymbol{v}$ are observable quantities, the subscript n represents the component of the

magnetic field $\boldsymbol{B}$ and of the velocity $\boldsymbol{v}$ normal to the surface S_p, whereas the subscript t represents the tangential component.

The magnetic helicity content of an active region at a specific time can be determined by integrating the helicity injection rate over time since its birth to the specified time, provided that no CME occurred which would have carried away helicity. According to Eq. (4), the magnetic helicity in an open volume can change either by the shuffling horizontal motions of field lines on the surface (first term, called shear term) or by the passage of twisted or sheared fields through the solar surface (second term, called emergence term).

Chae (2001) showed that when magnetic fields are normal to the surface, the flux distribution on the surface $\boldsymbol{B}_n$ can be exploited to determine the non-steady transverse motion of the field-line footpoints, and proposed to use the displacement velocity U_{LCT} determined by the technique of the local cross-correlation tracking (LCT) as a proxy for the transverse motion v_t. He also introduced a Fourier transform method for the fast computation of A_p from the B_n. Moreover, following Démoulin & Berger (2003), it is possible to write

$$U_{LCT} = v_t - \frac{v_n}{B_n} B_t, \tag{5}$$

and the photospheric helicity flux (or injection rate) simplifies to

$$\frac{dH}{dt} = -2 \int (\boldsymbol{U}_{LCT} \cdot \boldsymbol{A}_p) \boldsymbol{B}_n \, dS. \tag{6}$$

These equations put together the shear and emergence terms, as Démoulin & Berger (2003) realized that the emergence of a twisted flux system would cause what may appear as shear flows.

However, Pariat et al. (2005) showed that Eq. (6) introduces artificial signals because helicity flux densities per unit surface are not physical quantities. Therefore they presented a new estimation of helicity flux per unit of elementary magnetic flux. In this case the helicity flux is given by

$$\frac{dH}{dt} = -\frac{1}{2\pi} \int_S \int_{S'} \frac{dA(r)}{dt} B_n B'_n \, dS \, dS', \tag{7}$$

where $S = S'$ is the integration surface, $\frac{dA(r)}{dt}$ the relative rotation rate of pairs of photospheric positions defined by x and x', with $r = x - x'$. The use of the helicity flux density per unit of elementary magnetic flux permits us to reduce spurious signals.

The LCT method has some important practical advantages. First of all, it makes use of the line-of-sight magnetograms that are commonly available. Secondly, it is simple to implement, robust and flexible. However, it is possible to introduce large systematic errors into the results by not choosing interpolation algorithms with sufficient care (Potts et al. 2003) or by not choosing the correct size for the two input parameters of this method: FWHM (full width at half maximum) that defines the width of the apodizing window, and the time interval Δt between two images of comparison.

The accumulated magnetic helicity H_i (or total magnetic helicity injection) due to changes across the photospheric boundary can be determined by integrating the values of the helicity injection rate over the entire time interval Δt analyzed:

$$H_i = \int_0^{\Delta t} \frac{dH}{dt} dt. \tag{8}$$

Finally, indicating with Φ the average of the magnetic flux crossing the photosphere (given by $\Phi = 0.5\,\Phi_{pos} + 0.5\,|\Phi_{neg}|$), it is useful to evaluate the normalized helicity $|H_i|/\Phi^2$, which provides a measure of how much a magnetic configuration is stressed.

3. Data analysis

The method used to carry out our analysis can be described by the following steps: 1) selection (using SOHO/LASCO data) of halo CMEs; 2) search for the flare or eruptive filament closest in time for each selected CME; 3) attempt to identify the active region (AR) where the CME was initiated by means of a double cross-check based on the flaring-eruptive activity and the use of SOHO/EIT difference images; 4) determination of the magnetic flux trend, magnetic helicity injection rate dH/dt, accumulated magnetic helicity H_i and ratio $|H_i|/\Phi^2$ for the selected active regions.

More precisely, we selected a sample of halo CMEs from the SOHO/LASCO on-line catalog (http://cdaw.gsfc.nasa.gov/CME_list/). The choice to select halo CME is related to the fact that these events are generally initiated in areas located in the central part of the solar disk: this aspect is quite important when an analysis of line-of-sight magnetograms is carried out, because in this situation possible problems related to projection effects can be avoided. There were a total of 38 selected events in the time interval 2000 February 1st–2003 June 30; we show in Fig. 1a an example of a halo CME and the associated flare observed by SOHO/EIT in Fig. 1b.

We successively compared the time inferred by a back-extrapolation in time of the CME height-time trajectory with the time of the flare or filament eruption recorded in a time interval between one hour before and one hour after the CME, using the NOAA flare catalog (http://www.solarmonitor.org/index.php), in an attempt to obtain a first association between each CME and the corresponding flare or filament eruption.

In a next step, we used SOHO/EIT 171 Å images acquired during a time interval of two hours before and two hours after the CME occurrence and performed difference images between successive images to determine a possible increase or decrease of brightness. The double-cross check between the eruptive event registered in the NOAA report and the brightness variation inferred by the difference maps provided us a further indication about the active region that was the site of the initiation of the halo CME.

As an example, we show in Fig. 2a the EIT/SOHO image of the active region NOAA 10030 which was identified by the previously mentioned double check as the source region of the halo CME shown in Fig. 1a. Figure 2b shows the MDI/SOHO magnetogram relevant to NOAA 10030, acquired at 20:30 UT.

For some active regions that were very close to other active regions, it was not possible to draw the respective boundaries (e.g., NOAA 9114, NOAA 9393, NOAA 10069), therefore to avoid to neglect potentially significant flux that could influence the helicity flux measurements, we merged the above mentioned active regions with their neighboring ones (e.g., NOAA 9114+9115, NOAA 9393+9394, NOAA 10069 + 10077) and calculated the total helicity flux .

In order to minimize problems related to projection effects, we focused our attention on active regions located between ±35° of longitude from the central meridian. With this choice, we limited our analysis to 10 active regions and, correspondingly, to 12 CMEs, because both NOAA 10030 and 10365 were the source regions of two halo CMEs.

The halo CME events selected and the relevant active regions found by this method are reported in Table 1, where we can distinguish two classes of active regions: the first containing ARs giving rise to gradual halo CMEs, i.e. with positive acceleration (hereinafter called Class I) and the second relevant to ARs that

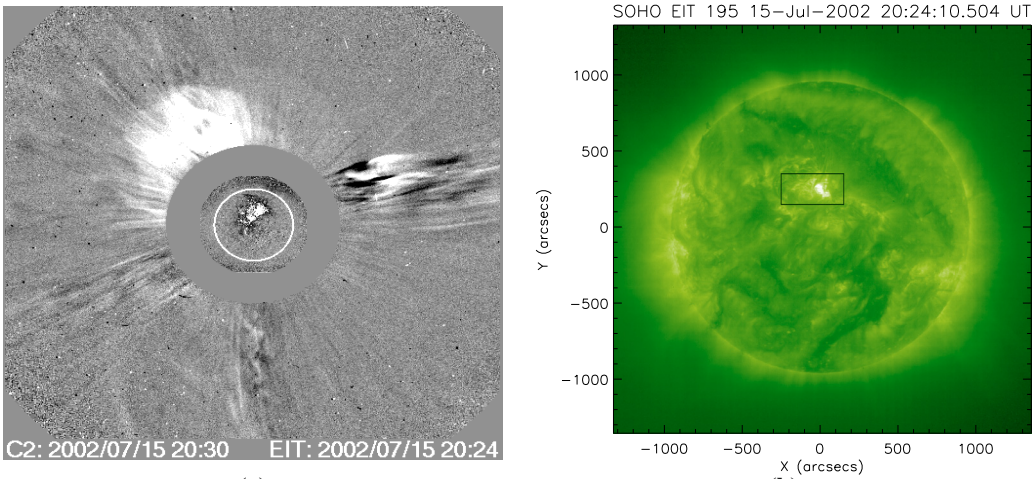

(a) **(b)**

Fig. 1. a) Difference image showing the halo CME observed by LASCO-C2 on 2002 july 15 at 20:30:05 UT, superposed on the EIT difference image relevant to 20:24 UT; **b)** SOHO/EIT full disk image acquired on 2002 july 15 at 20:24:10 UT, showing the location on the disk of the CME source region.

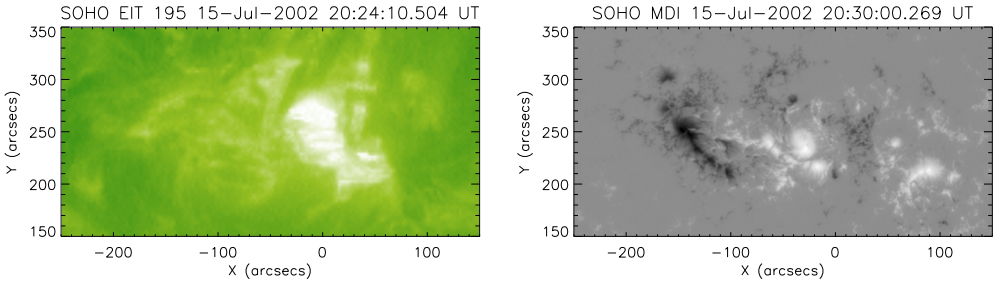

(a) **(b)**

Fig. 2. a) Zoom of the active region NOAA 10030 where the CME was initiated; the image was acquired by SOHO/EIT during the main phase of the flare; **b)** MDI/SOHO magnetogram showing the magnetic configuration of NOAA 10030 on 15 July 2002.

Table 1. Data on the halo CMEs and analyzed relevant eruptive events.

Day	CME time[a] (UT)	Linear speed (km s^{-1})	Acceleration (m s^{-2})	Gradual (g) or impulsive (i)	Associated event[b] (Beg, Max, End)UT	Active region NOAA number
2000-02-10	02:30:05	944	11.4	g	C7.3 (01:40, 02:08, 02:39)	8858
2000-04-10	00:30:05	409	2.5	g	M3.1 (23:26, 23:42, 23:55)	8948
2000-08-09	16:30:05	720	2.8	g	C2.3-ERU (15:19, 16:22, 17:00)	9114
2001-03-29	10:26:05	942	3.5	g	X1.7 (09:57, 10:15, 10:32)	9393
2001-04-10	05:30:00	2411	211.6	g	X2.3 (05:06, 05:26, 05:42)	9415
2002-07-15	20:30:05	1151	−25.6	i	X3.0 (19:59, 20:08, 20:14)	10030
2002-07-16	16:02:58	1636	−41.0	i	ERU (15:36, 15:39, 15:49)	10030
2002-08-16	12:30:05	1585	−67.1	i	M5.2-ERU (11:32, 12:32, 13:07)	10069
2002-10-25	15:06:05	870	−23.4	i	ERU (14:09, 14:11, 14:18)	10162
2002-12-19	22:06:05	1092	−36.2	i	M2.7 (21:34, 21:53, 22:17)	10229
2003-05-27	06:50:05	509	−14.6	i	M1.6 (05:06, 06:26, 07:16)	10365
2003-05-27	23:50:05	964	−9.6	i	X1.3 (22:56, 23:07, 23:13)	10365

Notes. The data on the halo CMEs and on the eruptive events were deduced from the SOHO/LASCO Catalog and the Active Region Monitor websites, respectively. [(a)] The CME time indicates the time of first appearance in LASCO/C2. [(b)] ERU indicates the occurrence of an erupting filament.

were sources of impulsive halo CMEs, i.e. characterized by negative acceleration (Class II).

We determined the magnetic flux evolution and the above mentioned parameters concerning the magnetic helicity injection for these two sets of active regions by means of MDI/SOHO low-resolution magnetograms taken with a 96 min cadence. We estimated the vertical field strength B_n by multiplying the MDI/SOHO line-of-sight component by $1/\cos\psi$, where ψ is the heliocentric angle.

We studied the magnetic evolution of each active region with respect to the time of the first observation of the CME in the LASCO/C2 field-of-view, which is considered below as the reference-time point. The collection of the line-of-sight magnetograms for each active region was carried out over a period of time that was chosen on the basis of the following two characteristics: 1) the time period expands over at least 24 h before and after the reference time; 2) during this time interval the longitude of the active region must be within ±35°.

We spatially aligned the sequence of magnetograms relevant to each active region by successive non-linear mapping, which takes into account the solar differential rotation effect.

Then we calculated the horizontal velocities of magnetic field lines at photospheric footpoints by measuring the local displacements of magnetic flux concentrations between two successive magnetograms with the LCT technique. We selected $FWHM = 10''$ and $\Delta t = 96$ min.

We used the method developed by Pariat et al. (2005) to estimate the magnetic helicity flux $\mathrm{d}H/\mathrm{d}t$ and to reduce spurious signals (see also Pariat et al. 2007, and references therein; Démoulin & Pariat 2009).

Then the accumulated amount of helicity H_i could be estimated by integrating the measured $\mathrm{d}H/\mathrm{d}t$ from the start of the observing run to a specific time. Finally, the total, positive and negative magnetic flux crossing the photosphere and the normalized helicity $|H_\mathrm{i}|/\Phi^2$ were computed.

3.1. Class I: gradual CMEs

In Fig. 3 we report the results obtained for two active regions related to gradual CMEs. Similar plots, concerning the other ARs belonging to the same Class, are reported in Fig. A.1 of Appendix A.

More specifically, the plots in Fig. 3 report the evolution of total, positive, and negative magnetic flux expressed in 10^{22} Mx (first row), helicity injection rate $\mathrm{d}H/\mathrm{d}t$ in 10^{42} Mx^2 h^{-1} (second row), accumulated helicity injection H_i in 10^{42} Mx^2 (third row), ratio $|H_\mathrm{i}|/\Phi^2$ (fourth row), positive ($\mathrm{H_+}$) and negative ($\mathrm{H_-}$) accumulated helicity injection (fifth row) for NOAA 8858 and NOAA 9415.

NOAA 8858 (Fig. 3, left panel): the total magnetic flux shows a very small decrease during the analyzed period (more precisely, the positive flux remains almost constant, while the negative flux slightly decreases). The helicity injection rate is generally negative, with the exception of few points with positive values. The accumulated helicity injection H_i shows a continuous increase (in absolute value), with a significant change in the curve slope *after* the CME event (third row). This change is also evident in the $|H_\mathrm{i}|/\Phi^2$ curve (fourth row), where it seems possible to distinguish two different regimes. The inspection of the graph shown in the fifth row, which gives the trend of the accumulated negative (asterisks) and positive (crosses) helicity injection, reveals that $\mathrm{H_-}$ increases and changes its trend after the CME occurrence, while $\mathrm{H_+}$ is very small and almost constant during the analyzed period. Note that the gradual CME was characterized by a velocity of 944 km s^{-1} and an acceleration of 11.4 m s^{-2}, and was associated with a C7.3 class flare.

NOAA 9415 (Fig. 3, right panel): the total magnetic flux is constant during the analyzed period, whereas the helicity injection rate shows alternating negative and positive values, with some more abrupt changes just before the CME. The accumulated helicity injection shows predominantly negative values prior to the CME occurrence and a successive rise to positive values after it. The ratio $|H_\mathrm{i}|/\Phi^2$ has a very irregular behavior, with a sudden change immediately before the CME and a clear increasing trend after it. The values of $\mathrm{H_-}$ and $\mathrm{H_+}$ show a very peculiar behavior, characterized by alternate phases where one component remains constant, while the other increases. Interestingly, one of the changes is temporarily correlated with the CME occurrence. The velocity and acceleration of the CME were 2411 km s^{-1} and 211.6 m s^{-2}, respectively, and the associated flare was of X2.3 class.

3.2. Class II: impulsive CMEs

Figure 4 shows the same parameters as in Fig. 3 for NOAA 10030 and 10069+10077, where impulsive CMEs occurred, while results concerning NOAA 10162, 10229 and 10365, belonging to the same Class, are reported in the Appendix (Fig. A.2).

NOAA 10030 (Fig. 4, left panel): during the analyzed period (five days), the total magnetic flux (as well as the positive and negative fluxes) shows a continuous increase, the helicity injection rate varies initially from positive to negative values and shows sudden changes in coincidence with the occurrence of two halo CMEs; in particular, after the second event, it again assumes positive values. H_i shows a continuous decrease after an initial increase to a maximum value of $\sim 2 \times 10^{42}$ Mx^2 h^{-1}, and an abrupt variation immediately after the second CME. However, when we look at the curve showing the ratio $|H_\mathrm{i}|/\Phi^2$ (fourth row), we notice that there is a very abrupt change immediately *before* the first CME and immediately *after* the second CME. The first change is due to the change in the sign of the accumulated helicity injection, while the latter might be explained by the changes in the trends of $\mathrm{H_-}$ and $\mathrm{H_+}$. In particular, concerning the trend of $\mathrm{H_-}$ and $\mathrm{H_+}$, reported in the fifth row, we can see that $\mathrm{H_-}$ is initially constant, then (some hours before the first CME) it starts to increase and this increase abruptly stops just before the second CME. The behavior of $\mathrm{H_+}$ is almost specular: it is increasing at the beginning of the period examined, then it stops (approximately when $\mathrm{H_-}$ starts to rise) and again suddenly starts to increase in coincidence with the CME (when $\mathrm{H_-}$ becomes constant). Note that the first CME, associated with an X3.0 class flare, was characterized by a velocity, as measured by LASCO C2, of 1151 km s^{-1} and a deceleration of 25.6 m s^{-2}, whereas the second CME had a velocity of 1636 km s^{-1}, a deceleration of 41.0 m s^{-2}, and was associated to an erupting filament.

NOAA 10069+10077 (Fig. 4, right panel): the magnetic flux shows an increase during the analyzed period, while the helicity injection rate (second row) is initially characterized by negative values and, after the CME occurrence, by positive values. This trend is reflected in the curve representing the accumulated helicity injection H_i, where the abrupt variation immediately *after* the CME is evident. The same behavior is shown by the $|H_\mathrm{i}|/\Phi^2$ values (fourth row). The graph shown in the fifth row shows that $\mathrm{H_-}$ and $\mathrm{H_+}$ have a similar trend to that observed for NOAA 10030: $\mathrm{H_-}$ initially increases while $\mathrm{H_+}$ remains constant and after the CME they invert their trends: $\mathrm{H_-}$ remains constant while $\mathrm{H_+}$ starts to increase. In this case, the CME velocity was 1585 km s^{-1}, the deceleration was 67.1 m s^{-2}, and the associated M5.2 flare was related to an erupting filament.

We note that the $|H_\mathrm{i}|/\Phi^2$ values obtained in our analysis for both Classes of CMEs are lower than those obtained by Démoulin & Pariat (2009): this is probably due to the limited time interval we used for the measurements of helicity accumulation, which in most of the cases excluded the emergence phase.

4. Discussion and conclusions

The role of magnetic helicity evolution in active regions producing eruptive events is considered to be very important and it is believed that the accurate measurement and modeling of the magnetic helicity is essential to understand the coupling between the photosphere, the corona and the heliosphere.

The study presented here was aimed at determining the temporal variations of magnetic flux and magnetic helicity injection in a sample of active regions generating halo CMEs, and how

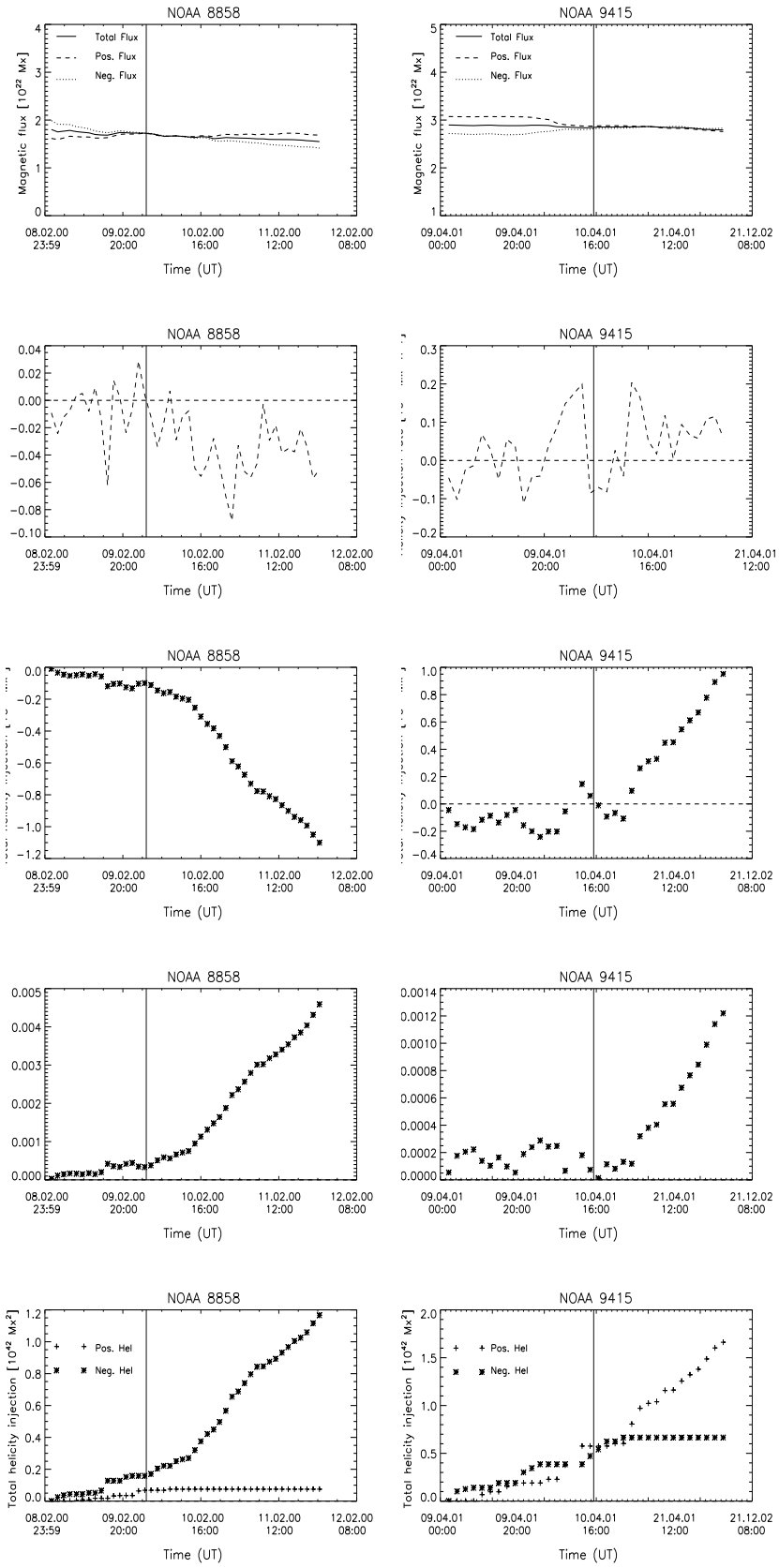

Fig. 3. *From top to bottom*: evolution of the magnetic flux (continuous line indicates the average total flux, marked line the positive flux and dotted line the negative flux), magnetic helicity injection rate, total helicity injection, ratio $|H_i|/\Phi^2$, positive H_+ and negative H_- accumulated helicity injection for ARs 8858, and 9415, belonging to Class I (gradual CMEs). Vertical lines indicate the time of the CME occurrence. Horizontal lines in the second and third rows indicate the zero values for the reported parameters.

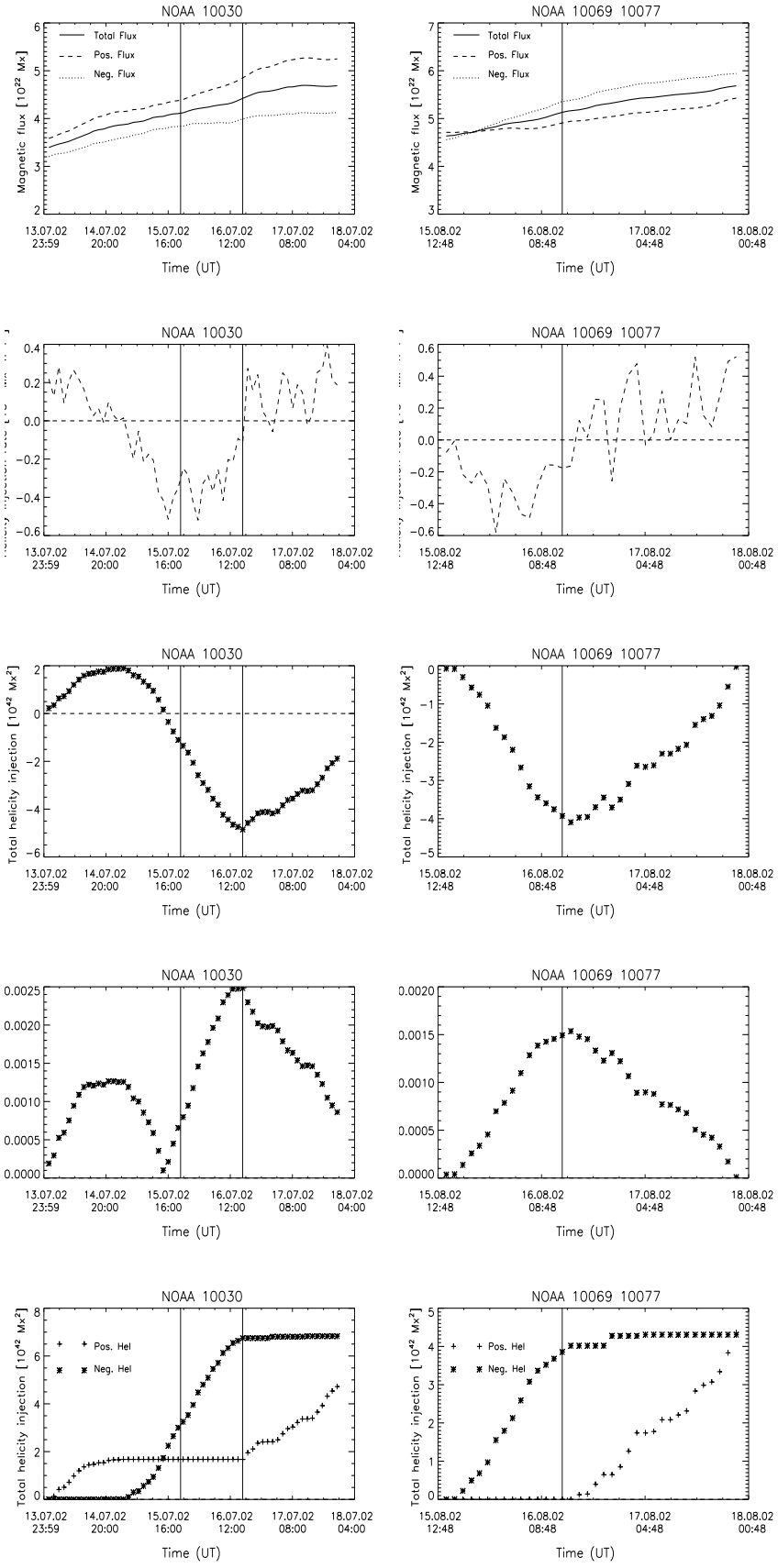

Fig. 4. Same as in Fig. 3 for ARs 10030 and 10069+10077, belonging to Class II (impulsive CMEs).

Table 2. Characteristics of the active regions, halo CMEs and analyzed relevant eruptive events.

NOAA	Latitude degrees	Event class	TMF[a]	HC[b]	TC[c]	ΔH_+ 10^{42} Mx^2	ΔH_- 10^{42} Mx^2
8858	+ 27	C7.3	slightly decreasing	yes	after	0.1	1.2
8948	−15	M3.1	slightly increasing	no	–	1.8	0.3
9114+9115	+ 12	C2.3-ERU	slightly increasing	yes	before	0	7
9393+9394	+ 20	X1.7	increasing (positive)	yes (small)	before	1	8.5
9415	−22	X2.3	constant	yes (great)	before and after	1.7	0.7
10030	+ 18	X3.0	increasing	yes	before	5	7
10030	+ 18	ERU	increasing	yes (great)	after	5	7
10069+10077	−8	M5.2-ERU	increasing	yes (great)	after	4	4.3
10162	+ 25	ERU	constant	yes (small)	before	9	0
10229	+ 15	M2.7	decreasing	no	–	0.2	3.5
10365	−6	M1.6	increasing	no	–	4.5	0.5
10365	−6	X1.3	constant	yes	after	4.5	0.5

Notes. [(a)] TMF: trend of the magnetic flux. [(b)] HC: Helicity change (slope of the curve). [(c)] TC: Time of change relative to the CME occurrence.

these variations could possibly be correlated with the CME occurrence.

We investigated the evolution of magnetic flux, magnetic helicity injection rate, and total magnetic helicity injection for ten active regions leading to twelve halo CMEs.

As a general result, we can deduce from the graphs shown in Figs. 3, 4, Figs. A.1, A.2 and from Table 2 that there is no unique behavior in magnetic helicity injection accompanying halo CME occurrence. In fact, in some cases there is an abrupt change in H_i correlated in time with the CME event (see, e.g., NOAA 8858, 9415, 10030 [second CME], 10069+10077, 10365 (second CME)), in others there is a slight change in the curve slope (NOAA 9114+9115, 9393+9394, 10162), and in some no significant variation is recorded (NOAA 8948, 10229, 10365 (first CME)). Therefore we cannot infer a general rule from this analysis.

We can, however, try to determine what conditions could give rise to these different behaviors and we discuss some possible relationships between the parameters characterizing the sample of ARs we analyzed.

A first conclusion that is possible to draw from the graphs shown in Figs. 3, 4 and Figs. A.1, A.2 is that the presence (or absence) of an abrupt change in H_i cannot be ascribed to the fact that the CME is gradual or impulsive: we actually found these changes in both classes (even if the most conspicuous H_i variations are associated with impulsive CMEs).

Nevertheless, an interesting result that can be deduced from the analysis of the total magnetic flux concerning the two classes is that the latter remains almost constant or shows a very slight increase for all the ARs that give rise to gradual CMEs, while it is significantly increasing or decreasing (with the exception of NOAA 10162) for impulsive CMEs. Moreover, on average the variation in helicity for the impulsive CMEs is more significant than for gradual CMEs. So the contribution in magnetic helicity injection due to flux emergence is quite significant also for more mature active regions, analogous to the results obtained by Tian & Alexander (2008) for new-born active regions.

In this regard, we recall that as already stated by other authors (see, e.g. Démoulin & Pariat 2009, and references therein), an increase of the magnetic flux, indicating the emergence of new flux tubes from the sub-photospheric layers, is the most important effect in causing the increase in the magnetic helicity flux. It is also possible that this emergence destabilizes the coronal magnetic configuration and leads to an eruptive event. On the basis of our results, we can conclude that this process was probably at work in some of the analyzed active regions, that is NOAA 9114+9115, NOAA 9393+9394 and NOAA 10030 (first CME), taking into account that in these active regions the change in magnetic helicity flux was observed *before* the CMEs. Note that these CME events are associated with X-class flares or erupting filaments.

Another effect, which causes a change in magnetic helicity flux *after* the CME, is related to a possible lack of torque balance between the subphotospheric and the coronal domain of a flux rope, which can occur once the CME has removed the accumulated stress in the magnetic field (Longcope & Welsh 2000; Chae et al. 2003; Petsov et al. 2003; Petsov et al. 2008).

The imbalance of magnetic torque can induce a transfer of helicity from the convective zone below the active region by torsional Alfvén waves, which is present until the coronal field has a torque large enough to balance the sub-photospheric torque.

Our analysis indicates that the observed change in the magnetic helicity flux occurred after the CMEs could be ascribed to this process for NOAA 8858, NOAA 9415, NOAA 10030 (second CME), NOAA 10069+10070 and probably also for NOAA 10365 (second CME).

However, in some of these cases, a flux emergence process also occurs, so it is not possible to state definitely what the main mechanism at work is. What we can notice from the trend of H_+ and H_- is though that for some of the active regions just mentioned these parameters show an alternate trend. In these active regions the cancellation of magnetic helicity should be taking place. Therefore it would be worthwhile to extend this study to other active regions that show a change in the magnetic helicity flux after a CME to obtain further information on this process.

Concerning NOAA 8948 and NOAA 10229, both characterized by decreasing magnetic flux and no change in the magnetic helicity trend both before and after the CME, we recall that also the photospheric shearing motions can be responsible for increasing the stress in the magnetic field. However, the new, less energetic configuration reached by these active regions after the eruptive events was probably not characterized by a torque imbalance as in the other cases. Interestingly, both events are associated with M-class flares, while the majority of the events quoted in the second category (i.e., those associated with the torque unbalance) are associated with X-class flares (characterized by a higher energy output than M-class flares) or with

erupting filaments, whose expulsion could greatly change the coronal magnetic configuration of the active region.

Another interesting result concerns the hemispheric helicity rule, which implies that H should be negative for ARs in the Northern hemisphere and positive for those in the Southern hemisphere (Seehafer 1990). Figures 3, 4, Figs. A.1, A.2 and Table 2 show that the analyzed ARs have a helicity accumulation in agreement with this rule, with the exception of NOAA 9415 and NOAA 10030 (showing both positive and negative H_i values during the analyzed time interval), 10069+10077 (showing negative helicity) and 10162 (characterized by positive helicity). Therefore 4/5 of the active regions of Class I have a helicity accumulation in agreement with the hemispheric helicity rule, while 3/5 of the active regions associated with impulsive CMEs seem to be related with an exception to this rule.

In conclusion, this study showed that magnetic helicity accumulation in our sample of active regions generating halo CMEs can exhibit significant changes when there are indications of new magnetic flux emergence. This emergence can change the helicity injection rate and also destabilize the coronal magnetic configuration, leading to an eruptive event.

Significant changes of the helicity injection rate can apparently also occur without the involvement of magnetic flux emergence. In most of these cases the observed changes follow the CME events and can be attributed to a process of restoring a torque balance between the subphotospheric and the coronal portion of the flux tubes.

Finally, we emphasize the result concerning the magnetic helicity injection with alternating sign found in those active regions where a considerable change of magnetic helicity was found, that was correlated in time with the CME occurrence. As in these active regions a cancellation of magnetic helicity should take place, we plan to further investigate this process both in these ARs as well in others, where a similar trend could be singled out.

Acknowledgements. The authors thank the anonymous referee for helpful comments and suggestions. This work was supported by the European Commission through the SOLAIRE Network (MTRN-CT-2006-035484), by the Istituto Nazionale di Astrofisica (INAF), by the Agenzia Spaziale Italiana (contract I/015/07/0) and by the Università degli Studi di Catania. The CME catalog is generated and maintained at the CDAW Data Center by NASA and The Catholic University of America in cooperation with the Naval Research Laboratory. SOHO is a project of international cooperation between ESA and NASA.

References

Alissandrakis, C. E. 1981, A & A, 100, 197
Antiochos, S. K., DeVore, C. R., & Klimchuk, J. A. 1999, ApJ, 510, 485
Archontis, V., & Török, T. 2008, A&A, 492, L38
Berger, T. E., & Lites, B. W. 2003, Sol. Phys., 213, 213
Berger, M. A. 1984, Geophys. Astrophys. Fluid. Dyn., 30, 79
Berger, M. A., & Field, G. B. 1984, J. Fluid Mech., 147, 133
Brandenburg, A. 2007, Highlights Astron., 14, 291
Brandenburg, A., & Sandin, C. 2004, A&A, 427, 13
Chae, J. 2001, ApJ, 560, L95
Chae, J., Moon, Y.-J., Rust, D. M., Wang, H., & Goode, P. R. 2003, JKoAS, 36, 33
Chen, J. 1996, J. Geophys. Res., 101, 27499
Chen, J., & Krall, J. 2003, J. Geophys. Res., 108, SSH 2-1
Chen, P. F., & Shibata, K. 2000, ApJ, 545, 524
Cook, G. R., Mackay, D. H., & Nandy, D., 2009, ApJ, 704, 1021
Démoulin, P., & Berger, M. A. 2003, Sol. Phys., 215, 203
Démoulin, P., & Pariat, E. 2009, Adv. Space Res., 43, 1013
Forbes, T. G. 2000, J. Geophys. Res., 105, 23153
Forbes, T. G., & Priest, E. R. 1995, ApJ, 446, 377
Heyvaerts, J., & Priest, E. R. 1984, A&A, 137, 63
Longcope, D. W., & Welsch, B. T. 2000, ApJ, 545, 1089
Longcope, D., Beveridge, C., Qiu, J., et al. 2007, Sol. Phys., 244, 45
Low, B. C. 1996, Solar Phys., 167, 217
Low, B. C., & Zhang, M. 2002, ApJ, 564, L53
Mackay, D. H., & van Ballegooijen, A. A. 2006, ApJ, 641, 577
MacQueen, R. M., & Fisher, R. R. 1983, Sol. Phys., 89, 89
Moon, Y. J., Chae, J., Wang, H., Choe, G. S., & Park, Y. D. 2002, ApJ, 580, 528
Nindos, A., & Andrews, M. D. 2004, ApJ, 616, L175
Nindos, A., Zhang, J., & Zhang, H. 2003, ApJ, 594, 1033
Pariat, E., Démoulin, P., & Berger, M. A. 2005, A&A, 439, 1191
Pariat, E., Nindos, A., Demoulin, P., & Berger, M. A. 2006, A&A, 452, 623
Pariat, E., Démoulin, P., & Nindos, A. 2007, Adv. Space Res., 39, 1706
Petsov, A. A. 2008, J. Astrophys. Astron., 29, 49
Petsov, A. A., Maleev, V. M., & Longcope, D. W. 2003, ApJ, 593, 1217
Potts, H. E., Barrett, R. K., & Diver, D. A. 2003, Sol. Phys., 217, 69
Priest, E. R., & Forbes, T. G. 1990, Sol. Phys., 126, 319
Qiu, J., Hu, Q., Howard, T. A., & Yurchyshyn, V. B. 2007, ApJ, 659, 758
Seehafer, N. 1990, Sol. Phys., 125, 219
Sheeley, N. R., Jr., Walters, J. H., Wang, Y.-M., & Howard, R. A. 1999, J. Geophys. Res., 104, 24739
Tian, L., & Alexander, D. 2008, ApJ, 673, 532
Yeates, A. R., & Mackay, D. H. 2009, ApJ, 699, 1024
Zuccarello, F. P., Soenen, A., Poedts, S., Zuccarello, F., & Jacobs, C. 2008, ApJ, 689, L157

Appendix A: Magnetic flux and magnetic helicity evolution

The plots in Figs. A.1 and A.2 report the evolution of total, positive, and negative magnetic flux expressed in 10^{22} Mx (first row), helicity injection rate dH/dt in 10^{42} $Mx^2\,h^{-1}$ (second row), accumulated helicity injection H_i in 10^{42} Mx^2 (third row), ratio $|H_i|/\Phi^2$ (fourth row), positive (H_+) and negative (H_-) accumulated helicity injection (fifth row) for NOAA 8948, 9114+9115 and 9393+9394, belonging to the Class I and for NOAA 10162, 10229 and 10365, belonging to Class II.

NOAA 8948 (Fig. A.1, leftt panel): the total, positive, and negative magnetic flux are slightly decreasing during the period analyzed. However, if we limit our attention to the time interval preceding the CME, we note a slight increase of both positive and negative magnetic fluxes. The helicity injection rate dH/dt (second row) is prevalently positive, with the exception of the last part of the analyzed period. The accumulated helicity injection (third row) is initially characterized by increasing positive values and in the last part of the analyzed period by a decreasing trend. The $|H_i|/\Phi^2$ ratio (fourth row) shows an increasing trend till the time of the corresponding increase in H_- (see the graph in the fifth row), but not correlated with the CME occurrence. The graph in the fifth row shows that the main contribution to the helicity injection is due to the increase of H_+, while there is an increase of H_- only during the last part of the analyzed period. The CME had a velocity of 409 km s^{-1}, an acceleration of 2.5 m s^{-2}, and was associated to an M3.1 flare.

NOAA 9114+9115 (Fig. A.1, middle panel): the total magnetic flux is slightly increasing during the analyzed period and in particular just before the CME occurrence; the helicity injection rate (second row), which is always characterized by negative values, shows an evident increasing trend before the CME occurrence (till the value of -0.4×10^{42} Mx^2) and a phase characterized by lower values (till -0.1×10^{42} Mx^2) *after* it. The accumulated helicity injection (third row) shows a different trend before and after the CME occurrence. This behavior is also evident in the curve showing the ratio $|H_i|/\Phi^2$. The graph reported in the fifth row indicates that the contribution to H_i is only due to H_-. Note that the CME had a velocity of 720 km s^{-1}, an acceleration of 2.8 m s^{-2} and it was associated with a C2.3 flare and an erupting filament.

NOAA 9393+9394 (Fig. A.1, right panel): the total magnetic flux shows an increase during the analyzed period (in this case, the positive flux increases, whereas the negative flux decreases); the helicity injection rate (second row) is predominantly characterized by negative values. The curve showing the accumulated helicity injection H_i indicates that there is a continuous increase of helicity, always characterized by negative values, also after the CME. Interestingly, the trend shows a slight variation a few hours before the CME. A similar trend is shown by the H_i/Φ^2 values (fourth row). The graph reported in the fifth row indicates that the main contribution to H_i is due to H_-, and that H_+ starts to increase some hours before the CME occurrence. In this case, the CME, associated to an X1.7 flare, had a velocity of 942 km s^{-1} and an acceleration of 3.5 m s^{-2}.

NOAA 10162 (Fig. A.2, left panel): the total magnetic flux is almost constant during the analyzed period (this is due to a smooth increase of the positive flux and to a contemporary decrease of the negative flux); the helicity injection rate shows a very spiky behavior, generally characterized by positive values. The accumulated helicity shows an almost monotonic increase, with a small plateau (reflecting the dH/dt value) at the CME occurrence. The ratio $|H_i|/\Phi^2$ shows an increasing trend with a similar plateau in coincidence with the CME occurrence. H_+ has a trend similar to H_i and $|H_i|/\Phi^2$, while H_- remains constant (assuming values very close to zero). In this case, the CME had a velocity of 870 km s^{-1}, a deceleration of 23.4 m s^{-2} and was associated with an erupting filament.

NOAA 10229 (Fig. A.2, middle panel): in this active region the total magnetic flux decreases during the analyzed period (the negative flux shows a stronger decrease than the positive flux), whereas the helicity injection rate generally shows negative values, with some abrupt changes to positive values. The accumulated helicity, and correspondingly the ratio $|H_i|/\Phi^2$ are monotonically increasing. In this case H_- (see the graph in the fifth row) shows a continuous increase, while H_+ has only a slight increase just before the CME occurrence and again some hours later. The velocity and deceleration of the CME were 1092 km s^{-1} and 36.2 m s^{-2}, respectively, and the associated flare was of M2.7 class.

NOAA 10365 (Fig. A.2, right panel): in the first row we can see that the total magnetic flux shows an evident increase during the analyzed period. However, a more careful inspection of this graph indicates that there is a clear increase before the first CME and almost no increase before the second CME. The helicity injection rate dH/dt is initially characterized by positive values and does not show significant variation after the first CME, while it changes, assuming also negative values, after the second CME. This behavior is clearly shown in the accumulated helicity (third row) and even more evidently in the $|H_i|/\Phi^2$ trend, especially as far as the second event is concerned. Similarly, H_+ (see the graph in the fifth row), which increases during the entire analyzed period, shows a small plateau after the second CME, and later starts to increase again, while H_-, which was almost zero until this event, starts to increase. The first CME had a velocity of 509 km s^{-1}, a deceleration of 14.6 m s^{-2}, and was associated with an M1.6 flare, while the second CME presented a velocity of 964 km s^{-1}, a deceleration of 9.6 m s^{-2}, and was associated with an X1.3 flare.

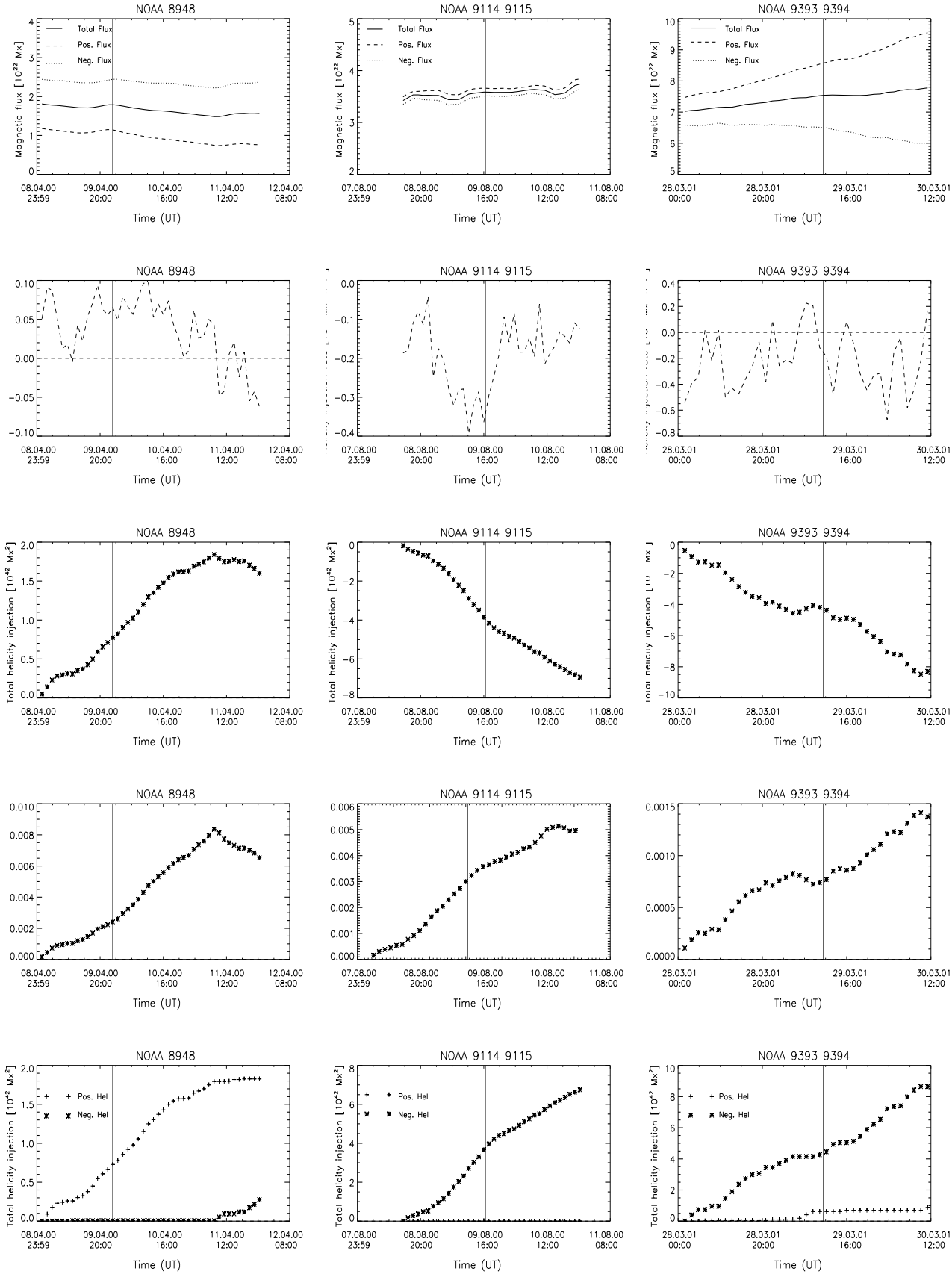

Fig. A.1. Same as in Fig. 3 for ARs 8948, 9114+9115 and 9393+9394, belonging to Class I (gradual CMEs).

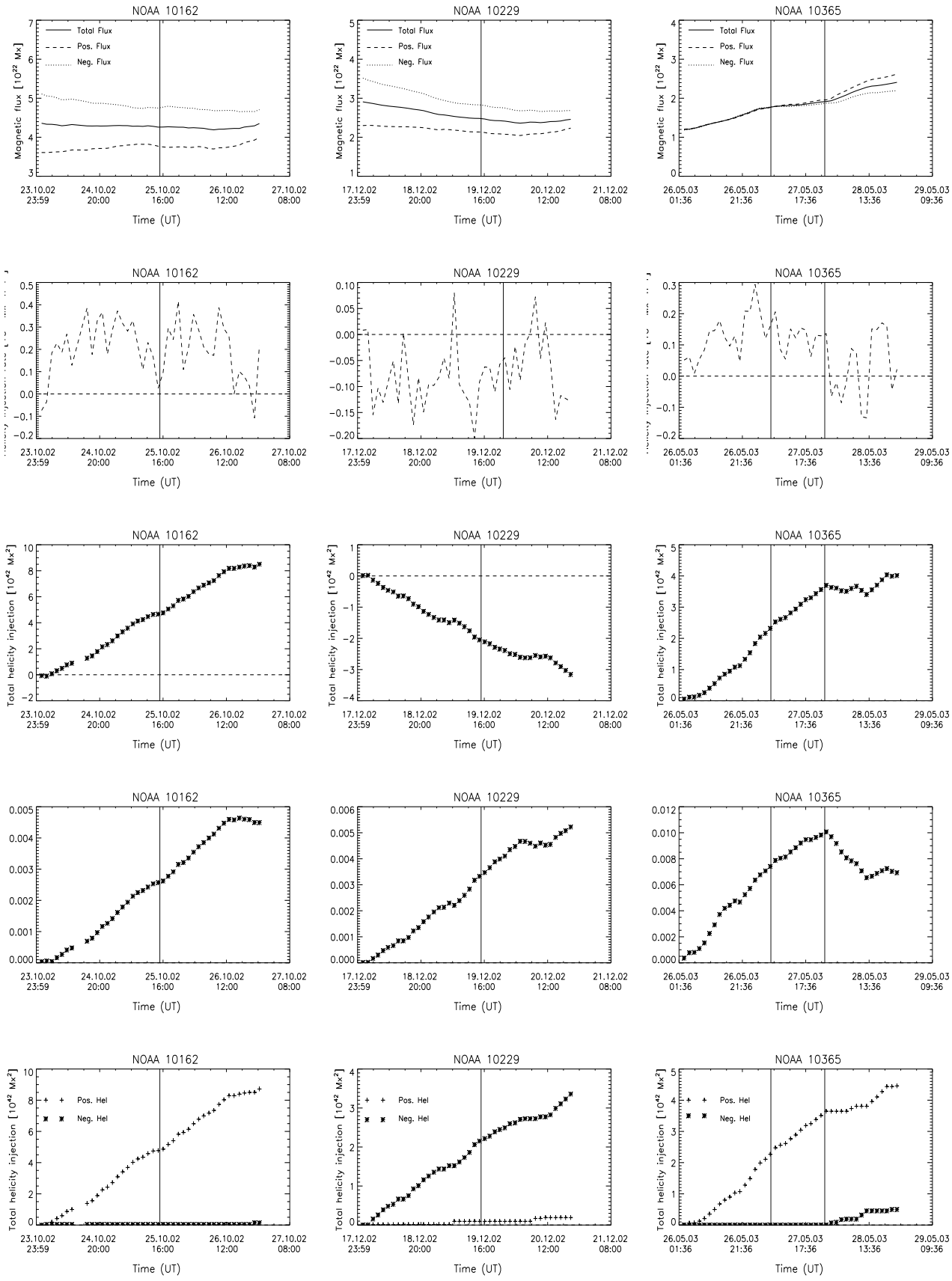

Fig. A.2. Same as in Fig. 3 for ARs 10162, 10229 and 10365, belonging to Class II (impulsive CMEs).